PHYSICAL REVIEW B VOLUME 15, NUMBER 2 15 JANUARY 1977

Frequency-dependent conductivity in multilayer assemblies

Michio Sugi and Sigeru Iizima
Electrotechnical Laboratory, Mukodai, Tanashi, Tokyo, Japan
(Received 1 June 1976)

The frequency behavior of conductivity in the multilayer assemblies as a hopping system have been studied by applying the extended Montroll-Weiss formalism. For "heterogeneous assemblies" consisting of different layers, a frequency dispersion is predicted as characteristic of each superstructure in layer sequence, while the "homogeneous assemblies" with identical layers are found to show a frequency-independent conductivity. The dispersion frequency, in contrast to that for the Maxwell-Wagner-type interface polarization, is immediately related to the transition rate of carriers traversing the individual layers. It is suggested that the precise information of electron transitions between localized states is obtainable by employing various heterogeneous structures realized as the actual assemblies of monomolecular layers.

I. INTRODUCTION

Multilayer assemblies can be constructed using the well-known Langmuir-Blodgett technique[1] by depositing an arbitrary number of monolayers (monomolecular sheets) one on top of the other. The elaboration of the technique recently attained by Kuhn and his co-workers, now known as the "molecular assembly technique,"[2] has realized various "heterogeneous assemblies" with deliberately designed sequences of different constituent layers as persistent structures[3] as well as usual Langmuir films or "homogeneous assemblies" consisting of identical layers.

Recent investigations on the electrical conduction in the molecular assemblies have indicated the existence of conductivity components governed by the superstructure of each assembly.[4-8] The model presented for such components is based on the hopping mechanism, allowing for the superstructure as a planar distribution of localized states at each interface between insulating layers.[6-8] Each constituent layer is then characterized with a single hopping rate for carriers at an energy level to traverse the layer. The rate is governed by the layer thickness l, the damping constant of wave function $\alpha(E)$, and the interface state density $N'(E)$, and expressed as

$$\lambda = \lambda(E, l) = \lambda_0[2\alpha(E)l]^{3/2} \exp\{-2\alpha(E)l - [4\alpha(E)/\pi N'(E) lkT]^{1/2}\}, \quad (1)$$

which has appropriately explained the dc conductivity of Cd salts of fatty acids[6-8] as well as the characteristic hump frequencies of photoconductivity dispersion observed in homogeneous and heterogeneous dye-sensitized assemblies.[4]

The present paper aims to show fundamental features of dispersive behaviors of such conductivity components predicted for the multilayer system within the framework of single rate scheme by application of the extended Montroll-Weiss formalism[9,10] (hereafter to be referred to as EMW). All expressions to be presented are those for infinite system to retain the analytical forms characterizing the fundamental features in physical contexts.

EMW is briefly reviewed in Sec. II together with its application for homogeneous assemblies whose conductivity is found to be frequency independent. Section III deals with heterogeneous assemblies, each of which is predicted to show a frequency dispersion characteristic of the corresponding superstructure in layer sequence. An explanation is also given for the better understanding of photoconductivity dispersion. In Sec. IV, we discuss the relevance of the predictions given in the preceding sections when they are applied for the actual assembly system inevitably associated with occasional inhomogeneities such as structural and compositional disorders or imperfections. Hopping rates are evaluated for Cd-salt layers of a few fatty acids easily available for assembly construction.

II. EMW FORMALISM AND ITS APPLICATION TO HOMOGENEOUS ASSEMBLIES

Scher and Lax[10] start from an application of the well-known fluctuation-dissipation theorem[11] to a system of noninteracting carriers obeying Boltzmann statistics and derive the expression of conductivity,

$$\sigma(\omega) = (e^2/kT) n D(\omega), \quad (2)$$

where n is the effective carrier concentration and

$$D(\omega) = \tfrac{1}{2}(i\omega)^2 \int_0^\infty \tfrac{1}{3}\langle[\vec{r}(t) - \vec{r}(0)]^2\rangle e^{-i\omega t} dt \quad (3)$$

is the Fourier transform of diffusion coefficient.

In Eq. (3), $\vec{r}$ is the position vector and the angular brackets denote the ensemble average, and the factor $\frac{1}{3}$ in the integrand is due to the projection of vector to the field direction. They then introduce the Montroll-Weiss formalism for continuous time random walk on a discrete lattice.[9] The carrier positions are now confined to the lattice points, every pair of which is characterized with a transition probability $\psi(\vec{s}, t)\Delta t$ that a flight of carrier occurs in the time interval $(t, t+\Delta t)$ resulting in a vector displacement $\vec{s}$.

By means of the set of ψ, s, Eq. (3) is rewritten[10]

$$D(\omega) = \frac{(i\omega)^2}{2} \frac{1-\tilde{\psi}(i\omega)}{i\omega} \frac{1}{3} \sum_{\vec{s}} s^2 \sum_{n=0}^{\infty} \tilde{R}_n(\vec{s}, i\omega), \quad (4)$$

where

$$\tilde{\psi}(i\omega) = \sum_{\vec{s}} \tilde{\psi}(\vec{s}, i\omega), \quad (5)$$

$$\tilde{\psi}(\vec{s}, i\omega) = \int_0^{\infty} \psi(\vec{s}, t) e^{-i\omega t} dt, \quad (6)$$

and $\tilde{R}_n(\vec{s}, i\omega)$ is the Fourier transform of the probability function for n steps and given as

$$\tilde{R}_n(\vec{s}, i\omega) = \sum_{\vec{s}_1} \sum_{\vec{s}_2} \cdots \sum_{\vec{s}_{n-1}} \tilde{\psi}(\vec{s}_1, i\omega) \times \tilde{\psi}(\vec{s}_2 - \vec{s}_1, i\omega) \cdots \tilde{\psi}(\vec{s} - \vec{s}_{n-1}, i\omega). \quad (7)$$

Let us consider our multilayer assemblies, in which carriers are confined in interfaces and only the flights to the neighboring interfaces are allowed. Equation (4) is then reduced to a one-dimensional case as

$$D(\omega) = \frac{(i\omega)^2}{2} \frac{1-\tilde{\psi}(i\omega)}{i\omega} \sum_{n=0}^{\infty} \xi_n^2 \quad (8)$$

and

$$\xi_n^2 = \sum_{x_1} \sum_{x_2} \cdots \sum_{x_{n-1}} \sum_{x} x^2 \tilde{\psi}(x_1, i\omega) \times \tilde{\psi}(x_2 - x_1, i\omega) \cdots \tilde{\psi}(x - x_{n-1}, i\omega). \quad (9)$$

For homogeneous assemblies with layer thickness l and transition rate λ, all interfaces are equivalent and associated with the probability function

$$\psi(x, t) = \lambda e^{-2\lambda t} \delta_{x, \pm l}, \quad (10)$$

and, therefore,

$$\tilde{\psi}(x, i\omega) = [\lambda/(2\lambda + i\omega)] \delta_{x, \pm l}. \quad (11)$$

The n-fold sum in Eq. (9) is reduced as

$$\xi_n^2 = \langle x_n^2 \rangle_{\text{av}} [\tilde{\psi}(i\omega)]^n, \quad (12)$$

where $\langle x_n^2 \rangle_{\text{av}}$ is the mean-square displacement after n steps and given in this case as,[12]

$$\langle x_n^2 \rangle_{\text{av}} = nl^2. \quad (13)$$

Using Eqs. (12) and (13), Eq. (8) yields a frequency-independent coefficient

$$D(\omega) = l^2 \lambda, \quad (14)$$

which is equivalent to the expression of dc conductivity given in the previous papers[6-8] except for the difference of factor 2 due to the different assumption adopted in the present EMW scheme.[13]

III. HETEROGENEOUS ASSEMBLIES AND DISPERSION PHENOMENA

The general expression for heterogeneous assemblies has rather a complicated form. Let m be the number of classes of inequivalent interfaces, then each $\tilde{\psi}(x, i\omega)$ in Eq. (9) should be replaced by an $m \times m$ matrix $\tilde{\Psi}(x, i\omega)$. Consequently, Eq. (9) is now an operator acting upon a ket vector $\vec{f}^T = (f_1, f_2, \ldots, f_m)$ representing the equilibrium carrier distribution with a condition $\sum f_i = 1$, while $[1 - \tilde{\psi}(i\omega)]/i\omega$ in Eq. (8) should be replaced by a bra vector $[\vec{1} - \tilde{\Psi}(i\omega)]/i\omega = (1 - \tilde{\psi}_1, 1 - \tilde{\psi}_2, \ldots, 1 - \tilde{\psi}_m)/i\omega$ denoting the probability that a carrier stays in an interface belonging to either of the different classes.

Let us consider a heterogeneous assembly constructed by the alternate deposition of two different layers (1) and (2), each characterized with l_1, λ_1 or l_2, λ_2. As shown in Fig. 1(a), the layer sequence -(1)-(2)-(1)-(2)- is associated with the interface sequence -[1]-[2]-[1]-[2]-, and the corresponding expressions are

$$\tilde{\Psi}(x, i\omega) = \frac{1}{\lambda_1 + \lambda_2 + i\omega} \times \begin{pmatrix} 0 & \lambda_1 \delta_{x, l_1} + \lambda_2 \delta_{x, -l_2} \\ \lambda_1 \delta_{x, -l_1} + \lambda_2 \delta_{x, l_2} & 0 \end{pmatrix}, \quad (15)$$

$$\vec{f} = \frac{1}{2} \begin{pmatrix} 1 \\ 1 \end{pmatrix}, \quad (16)$$

$$[\vec{1} - \tilde{\Psi}(i\omega)]/i\omega = (\lambda_1 + \lambda_2 + i\omega)^{-1}(1, 1), \quad (17)$$

and

$$x^2 = \{[r_1(+) - r_1(-)] l_1 + [r_2(+) - r_2(-)] l_2\}^2, \quad (18)$$

where $r_1(\pm)$ and $r_2(\pm)$ are the numbers of steps with displacements $\pm l_1$ and $\pm l_2$, respectively, and therefore

$$n = r_1(+) + r_1(-) + r_2(+) + r_2(-). \quad (19)$$

Equations (15)–(19) will lead to a rigorous solution of conductivity. However, it lies beyond the scope of the present paper to show the rigorous but too

-(1)-(2)-(1)-(2)-(1)-(2)- LAYER SEQUENCE

λ_1 λ_2 λ_1 λ_2 λ_1 λ_2 TRANSITION RATE

-(1)-(2)-(1)-(2)- INTERFACE SEQUENCE

(a)

-(2)-(1)-(1)-(2)-(2)-(1)- LAYER SEQUENCE

λ_2 λ_1 λ_1 λ_2 λ_2 λ_1 TRANSITION RATE

-(1)-(2)-(3)-(4)- INTERFACE SEQUENCE

(b)

FIG. 1. Examples of heterogeneous assemblies consisting of two different layers (1) and (2), each associated with the transition rate λ_1 or λ_2. (a) The layers (1) and (2) are alternately deposited; (b) alternate stacking of the layer pairs (1)-(1) and (2)-(2).

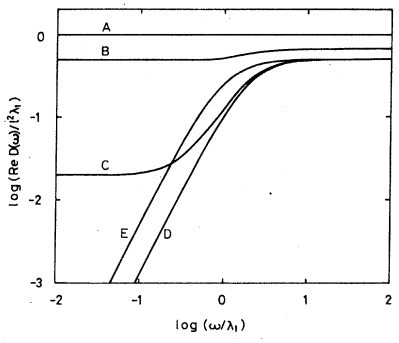

FIG. 2. Normalized plot of $\mathrm{Re}D(\omega)$ vs ω for heterogeneous assemblies with layer sequences -(1)-(2)- (A-D) and -(1)-(1)-(2)-(2)- (E) with $\lambda_2/\lambda_1 = 1$ (A), $\frac{1}{3}$ (B), $\frac{1}{100}$ (C), and 0 (D and E).

much complicated solution. If we put $l_1 = l_2 = l$, the above expressions are readily simplified as

$$\xi_n^2 = \sum_{r=0}^{\infty} \langle x_{n,r}^2 \rangle_{\mathrm{av}} \frac{n!}{r!(n-r)!} \frac{\lambda_1^r \lambda_2^{n-r}}{(\lambda_1+\lambda_2+i\omega)^n} \tag{20}$$

and

$$\langle x_{n,r}^2 \rangle_{\mathrm{av}} = \begin{cases} l^2 + 4rl^2(1-r/n) & \text{for } n \text{ odd}, \\ 4rl^2[1-(r-1)/(n-1)] & \text{for } n \text{ even}, \end{cases} \tag{21}$$

which lead to the diffusion coefficient expressed as

$$D(\omega) = \frac{l^2}{2}\left(\frac{4\lambda_1\lambda_2}{\lambda_1+\lambda_2} + \frac{(\lambda_1-\lambda_2)^2}{\lambda_1+\lambda_2}\frac{i\omega}{2(\lambda_1+\lambda_2)+i\omega}\right). \tag{22}$$

As shown in Fig. 2, Eq. (22) exhibits a frequency dependence unless $\lambda_1 = \lambda_2$, in which case the second term vanishes, coinciding with Eq. (14) as a matter of course. For $\lambda_1 \gg \lambda_2$, the real part is

$$\mathrm{Re}D(\omega) \cong l^2\left(2\lambda_2 + \frac{\lambda_1}{2}\frac{(\omega/2\lambda_1)^2}{1+(\omega/2\lambda_1)^2}\right). \tag{23}$$

showing that the conductivity is approximated as a sum of two components, each governed by either of two rates. The first term gives the dc level dependent on the slower rate λ_2. The second component is a Debye-type term to exhibit a dispersion hump around $2\lambda_1$. This dispersion term shows an apparent similarity to that to be due to the Maxwell–Wagner-type interface polarization in an analogous structure composed of the layers of dielectric media (1) and (2), each characterized with the dielectric constant ϵ_1 or ϵ_2 and the conductivity σ_1 or σ_2.[14] The characteristic frequency is in this case governed by those macroscopic physical constants as $\sigma_1/(\epsilon_1+\epsilon_2)$, if $\sigma_1 \gg \sigma_2$.

The dispersion frequency due to the present scheme is, however, distinguishable from the Maxwell-Wagner effect, since this is dependent also on the interface sequence of the assembly, while the Maxwell-Wagner scheme predicts the invariance of over-all impedance to the sequence of elements connected in series. Let us consider another sequence -(1)-(1)-(2)-(2)-, which should be equivalent to the above examined case as for the Maxwell-Wagner effect. For simplicity, we put $\lambda_2 = 0$ besides $l_1 = l_2$, since the dispersion term is now to be questioned. The interfaces are categorized into four classes as shown in Fig. 1(b) with the interface sequence -[1]-[2]-[3]-[4]-. The corresponding expressions are

$$\tilde{\Psi}(x, i\omega) = \begin{bmatrix} 0 & [\lambda_1/(2\lambda_1+i\omega)]\delta_{x,-l} & 0 & 0 \\ [\lambda_1/(\lambda_1+i\omega)]\,\delta_{x,l} & 0 & [\lambda_1/(\lambda_1+i\omega)]\,\delta_{x,-l} & 0 \\ 0 & [\lambda_1/(2\lambda_1+i\omega)]\,\delta_{x,l} & 0 & 0 \\ 0 & 0 & 0 & 0 \end{bmatrix}, \tag{24}$$

$$\vec{f} = \frac{1}{4}\begin{bmatrix}1\\1\\1\\1\end{bmatrix}, \tag{25}$$

and

$$[\vec{1} - \vec{\psi}(i\omega)]/i\omega = ((\lambda_1 + i\omega)^{-1}, (2\lambda_1 + i\omega)^{-1}, (\lambda_1 + i\omega)^{-1}, (i\omega)^{-1}). \tag{26}$$

The nonzero displacements are,

$$x^2 = \begin{cases} 4l^2 & \text{for [1]-[3] and [3]-[1]}, \\ l^2 & \text{for [1]-[2], [2]-[1],} \\ & \text{[1]-[3], and [3]-[1]}. \end{cases} \tag{27}$$

The diffusion coefficient is obtained after a straightforward calculation as

$$D(\omega) = \tfrac{1}{2} l^2 \lambda_1 i\omega/(\lambda_1 + i\omega), \tag{28}$$

with the real part

$$\mathrm{Re}D(\omega) = \tfrac{1}{2} l^2 \lambda_1 \frac{(\omega/\lambda_1)^2}{1 + (\omega/\lambda_1)^2}, \tag{29}$$

which is clearly different from the case (a) characterized with Eq. (23), since for this case (b) the dispersion frequency is no more $2\lambda_1$ but λ_1, as shown in Fig. 2.

Any restriction of flight motion of carriers to a localized region will result in a frequency-dependent conductivity.[10] The above examined cases (a) and (b) represent the structural restrictions due to the heterogeneous layer sequences. Even in homogeneous assemblies, dispersion phenomena are expected for photoconductivity within the present scheme in accordance with the experimental results.[4] The excitable carriers move under illumination either with the high-energy rate λ_h or with the low-energy rate λ_l, each given by Eq. (1). The carrier motion with the high-energy rate should be rather strongly restricted by the generation-recombination process, since the steady-state carrier distribution is far apart from that in the dark thermal equilibrium.

Let us consider a simplified model in which the fractions a and $1-a$ of excitable carriers are at the high-energy level and the low-energy level, respectively, and this fractional distribution is restored immediately after each flight event. For this case, the probability function can be written

$$\tilde{\psi}(i\omega) = a\frac{2\lambda_h}{2\lambda_h + i\omega} + (1-a)\frac{2\lambda_l}{2\lambda_l + i\omega}. \tag{30}$$

Using Eq. (30) together with Eqs. (8), (12) and (13), the diffusion coefficient is readily evaluated as

$$D(\omega) = \frac{l^2}{(1-a)\lambda_h + a\lambda_l} \times \left(\lambda_h\lambda_l + a(1-a) \times (\lambda_h - \lambda_l)^2 \frac{i\omega}{2(1-a)\lambda_h + 2a\lambda_l + i\omega}\right), \tag{31}$$

which is associated with a dispersion term unless $a = 0$ or 1. For the realistic case, $a \gtrsim 0$ and $\lambda_h \gg \lambda_l$, the photoincrement of the real part is approximated as a Debye term governed by $2\lambda_h$ as

$$\mathrm{Re}[D(\omega) - D(\omega)|_{a=0}] \cong al^2\lambda_h \frac{(\omega/2\lambda_h)^2}{1 + (\omega/2\lambda_h)^2}. \tag{32}$$

In this model, the recombination range can be evaluated as the layer thickness multiplied with the square root of the average number of the high-energy flights occurring successively. The recombination range is therefore estimated as

$$l_r = l\left(\sum_{n=1}^{\infty} na^{n-1}(1-a)\right)^{1/2} = \frac{l}{(1-a)^{1/2}}, \tag{33}$$

referring to Eq. (13), which is consistent with the assumption that the fractional distribution is restored immediately after the flight event.

If the fractional distribution is very slowly attained, however, two energy levels should be rather independently dealt with, each associated with a or $1-a$ fraction of the excitable carriers. In this extreme case, the recombination range tends to infinity and the diffusion coefficient can be evaluated as a sum of two frequency-independent components as

$$D(\omega) = al^2\lambda_h + (1-a)l^2\lambda_l. \tag{34}$$

It should be emphasized that between two extreme cases discussed above, the frequency behavior of photoconductivity generally depends on the generation-recombination process. This is important for actual application of the present scheme to a system, since the dependence will allow in turn the characterization of the process in itself.

IV. DISCUSSION

In Secs. I–III, the frequency behaviors of diffusion coefficient have been predicted for various assemblies. The constituent layers have been assumed to be "perfect" layers, each characterized with a unique transition rate λ for a given energy level.

Let us consider the actual monolayers which are inevitably associated with occasional structural and compositional imperfections. As discussed

in Ref. 7, the influence of imperfections is smeared out, resulting in a unique rate given by Eq. (1) for the average layer thickness, if the average size of imperfections is far smaller than the corresponding hopping domain defined as a range within which an electron is likely to find a state to hop into. If the imperfections are the large scale patches covering many hopping domains, however, the rate is subjected to local fluctuation and the intrainterface motion of carriers must be explicitly allowed for as well as the interinterface flights.

Let λ, λ', λ_t, and l_t^2 be the interinterface flight rate of normal region, that of anomalous patches, the intrainterface rate and its average square displacement, respectively, then the local regions of interface are categorized into three classes as shown in Fig. 3, each associated with either of three sets of the probability functions,

$$\begin{aligned}
&\tilde{\psi}_1(i\omega)_\perp = 2\lambda/[2(\lambda_t+\lambda)+i\omega],\\
&\tilde{\psi}_1(i\omega)_\parallel = 2\lambda_t/[2(\lambda_t+\lambda)+i\omega] \quad \text{for (1)-(1)},\\
&\tilde{\psi}_2(i\omega)_\perp = (\lambda+\lambda')/(2\lambda_t+\lambda+\lambda'+i\omega),
\end{aligned} \tag{35a}$$

$$\tilde{\psi}_2(i\omega)_\parallel = 2\lambda_t/(2\lambda_t+\lambda+\lambda'+i\omega) \tag{35b}$$

for (1)-(2) and (2)-(1),

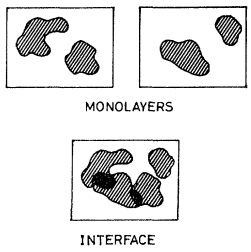

FIG. 3. Schematic representation of interface with imperfections. Monolayers with normal regions (1) and anomalous patches (2) (upper figures) form an interface associated with three different classes of local regions: (1) normal regions on both sides, (1)-(1); (2) an anomalous patch on one side, (1)-(2) and (2)-(1); (3) anomalous patches on both sides, (2)-(2).

and

$$\begin{aligned}
&\tilde{\psi}_3(i\omega)_\perp = 2\lambda'/[2(\lambda_t+\lambda')+i\omega],\\
&\tilde{\psi}_3(i\omega)_\parallel = 2\lambda_t/[2(\lambda_t+\lambda')+i\omega] \quad \text{for (2)-(2)},
\end{aligned} \tag{35c}$$

where $\tilde{\psi}_i(i\omega)_\parallel$ and $\tilde{\psi}_i(i\omega)_\perp$ are the sums of $\tilde{\psi}_i(x,i\omega)$'s for intra- and interinterface flights, respectively. Let p be the fraction of anomalous area, the configurational average of the interinterface-flight probability function can be written

$$\begin{aligned}
\langle\tilde{\psi}(i\omega)\rangle = {}& [p^2\tilde{\psi}_1(i\omega)_\perp + 2p(1-p)\tilde{\psi}_2(i\omega)_\perp + (1-p)^2\tilde{\psi}_3(i\omega)_\perp]\\
&\times\sum_{n=0}^{\infty}\sum_{r_1=0}^{n}\sum_{r_2=0}^{n-r_1}\frac{n!}{r_1!r_2!(n-r_1-r_2)!}[p^2\tilde{\psi}_1(i\omega)_\parallel]^{r_1}[2p(1-p)\tilde{\psi}_2(i\omega)_\parallel]^{r_2}[(1-p)^2\tilde{\psi}_3(i\omega)_\parallel]^{n-r_1-r_2},
\end{aligned} \tag{36}$$

if the average patch area is far smaller than $l_t^2\lambda_t/\lambda'$. Further, if we assume $\lambda_t \gg \lambda, \lambda'$, the above expression is approximated as

$$\langle\tilde{\psi}(i\omega)\rangle \cong 2\bar{\lambda}/(2\bar{\lambda}+i\omega), \tag{37}$$

where $\bar{\lambda}$ is the average defined as

$$\bar{\lambda} = p\lambda' + (1-p)\lambda. \tag{38}$$

It is suggested that the single rate scheme remains valid even for monolayers with large scale imperfections, since the above conditions are likely fulfilled because of the very large value of $l_t^2\lambda_t/l^2\lambda = \mu_\parallel/\mu_\perp$ as suggested by Lundström, Löfgren, and Stenberg,[15] who have estimated $\mu_\parallel/\mu_\perp \sim 2\times10^7$ for stearate monolayers. Using this value and $l^2 \sim 5\times10^{-14}$ cm^2, we obtain a very tolerant condition $l_t^2\lambda_t/\lambda' \sim (\lambda/\lambda')\times10^{-6}$ cm^2 as representing the critical patch size to violate the single rate scheme.

It will be easily understood that Eq. (38) leads to the same expression of conductivity as that for homogeneous assemblies of inhomogeneously mixed monolayers presented in Ref. 7,

$$\sigma \sim \bar{\sigma} = p\sigma_1 + (1-p)\sigma_2 \tag{39}$$

if we recognize $l^2 \cong \langle l^2\rangle_{\text{av}} \cong \langle l\rangle_{\text{av}}^2$, where σ_1, p and $\sigma_2, 1-p$ are the conductivities and the molar fractions of the corresponding pure monolayers, respectively.

In the case of photoconduction, however, the above discussion may not be applicable, since the generation-recombination process should restrict also the intrainterface motion. If each electron at the high energy level has a recombination range far smaller than the patch size, the averaged function can be rather written

$$\langle\tilde{\psi}_h(i\omega)\rangle = p^2\tilde{\psi}_{h1}(i\omega)_\perp\sum_{n=0}^{\infty}[\tilde{\psi}_{h1}(i\omega)_\parallel]^n + 2p(1-p)\tilde{\psi}_{h2}(i\omega)_\perp\sum_{n=0}^{\infty}[\tilde{\psi}_{h2}(i\omega)_\parallel]^n + (1-p)^2\tilde{\psi}_{h3}(i\omega)_\perp\sum_{n=0}^{\infty}[\tilde{\psi}_{h3}(i\omega)_\parallel]^n, \tag{40}$$

where the suffix h refers to the high-energy level. Equation (40) is reduced to a linear combination of three different rate processes,

$$\langle\tilde{\psi}_h(i\omega)\rangle = p^2\tilde{\psi}_{h1}(i\omega) + 2p(1-p)\tilde{\psi}_{h2}(i\omega) + (1-p)^2\tilde{\psi}_{h3}(i\omega), \tag{41}$$

where

$$\tilde{\psi}_{h1}(i\omega) = 2\lambda_{h1}/(2\lambda_{h1} + i\omega), \quad (42a)$$

$$\tilde{\psi}_{h2}(i\omega) = (\lambda_{h1} + \lambda_{h2})/(\lambda_{h1} + \lambda_{h2} + i\omega), \quad (42b)$$

and

$$\tilde{\psi}_{h3}(i\omega) = 2\lambda_{h2}/(2\lambda_{h2} + i\omega). \quad (42c)$$

However, the low-energy rate can be evaluated within the single rate scheme by using Eq. (38), and the probability function is written

$$\langle \tilde{\psi}_l(i\omega) \rangle = 2\bar{\lambda}/(2\bar{\lambda}_l + i\omega). \quad (43)$$

Equations (40)–(43), as is easily understood, will yield a diffusion coefficient associated with three dispersion terms by applying a treatment similar to that for Eqs. (30)–(31) in Sec. III.

In the case of photoconduction, therefore, the presence of large scale imperfections may violate the single rate scheme, with the local high-energy rates being preserved. This consideration supports the actual situation that the dark dispersion phenomena are more difficult to observe than the photoeffects, since the higher quality of monolayers are required for the successful dark measurements. The dark behaviors are indispensable for the precise analyses of electron transports under various conditions, since they characterize the transport near the thermal equilibrium as representing the reference to other conditions.

As for the dark state, the transition rates can be estimated using the dc conductivity data so far obtained[6-8]; they are 10^{-1}–10^{-2}, 10^{-2}–10^{-3}, and around 10^{-4} Hz for Cd-palmitate, Cd-stearate, and Cd-arachidate, respectively, at liquid-nitrogen temperature. Among these conventionally used monolayers, the combination of palmitate and arachidate will be hopeful for the actual observation. The difference of rates by two decades or more will be sufficient for dispersive behaviors to be discernible as seen in Fig. 2.

It should be noted that the ac measurements of dark and photoconductivities followed by the analyses after the present scheme, if applied to various assemblies, will allow to obtain precise information of electronic states in organic molecules and the electron transition processes between them.

ACKNOWLEDGMENTS

The authors wish to thank Dr. H. Okushi for his helpful discussion. They are also indebted to Professor H. Kuhn and Dr. D. Möbius for their valuable comments in the early stage of the work.

[1] K. B. Blodgett, J. Am. Chem. Soc. 57, 1007 (1935).
[2] For a comprehensive review, see H. Kuhn, D. Möbius, and H. Bücher, in *Techniques of Chemistry*, edited by A. Weissberger and B. W. Rossiter (Wiley, New York, 1973), Vol. 1, Part III B.
[3] A. Matsuda, M. Sugi, T. Fukui, S. Iizima, M. Miyahara, and Y. Otsubo, J. Appl. Phys. (to be published).
[4] M. Sugi, K. Nembach, D. Möbius, and H. Kuhn, Solid State Commun. 15, 1867 (1974).
[5] M. Sugi, K. Nembach, and D. Möbius, Thin Solid Films 27, 205 (1975).
[6] M. Sugi, T. Fukui, and S. Iizima, Appl. Phys. Lett. 27, 559 (1975); see also 28, 240 (1976).
[7] S. Iizima and M. Sugi, Appl. Phys. Lett. 28, 548 (1976).
[8] M. Sugi, T. Fukui, and S. Iizima, Chem. Phys. Lett. (to be published).
[9] E. W. Montroll and G. H. Weiss, J. Math. Phys. 5, 167 (1965).
[10] H. Scher and M. Lax, Phys. Rev. B 7, 4502 (1973).
[11] R. Kubo, J. Phys. Soc. Jpn. 12, 570 (1957).
[12] S. Chandrasekhar, Rev. Mod. Phys. 15, 1 (1943).
[13] In Refs. 6–8, each interface was assumed to be connected to either of the neighboring interfaces (one-channel connection), leading to twice as small conductivity as that derived from Eq. (14) for the two-channel connection case. The validity of the previous papers is not affected by the factor 2, which is considerably smaller than the deviation of conductivity data so far obtained, although the two-channel connection should be rather the more proper model of actual multilayers.
[14] W. F. Brown, Jr., in *Handbuch der Physics*, edited by S. Flügge (Springer, Berlin, 1956), Vol. XVII.
[15] I. Lundström, H. Löfgren, and M. Stenberg, Solid State Commun. 18, 457 (1976).